A Comprehensive Framework for Tracking Control and Thrust Allocation for a Highly Over-Actuated Autonomous Surface Vessel

Matthew G. Feemster,
Systems Engineering Department
U.S.Naval Academy
Annapolis, MD 21402
feemster@usna.edu

Joel M. Esposito
Systems Engineering Department
U.S.Naval Academy
Annapolis, MD 21402
esposito@usna.edu

Abstract

In this paper, we present a comprehensive trajectory tracking framework for cooperative manipulation scenarios involving marine surface ships. Our experimental platform is a small boat equipped with six thrusters, but the technique presented here can be applied to a multi-ship manipulation scenario such as a group of autonomous tugboats transporting a disabled ship or unactuated barge. The primary challenges of this undertaking are: (1) the actuators are unidirectional and experience saturation; (2) the hydrodynamics of the system are difficult to characterize; and (3) obtaining acceptable performance under field conditions (i.e., GPS errors, wind, waves, etc) is arduous.

To address these issues, we present a frame work that includes trajectory generation, tracking control, and force allocation that, despite actuator limitations, results in asymptotically convergent trajectory tracking. In addition, the controller employs an adaptive feedback law to compensate for unknown – difficult to measure – hydrodynamic parameters. Field trials are conducted utilizing a 3 meter vessel in a nearby creek.

1 Introduction

In this paper we present a control framework that allows a highly overactuated marine vessel to track a reference trajectory. The major contribution of our framework is that each facet is constructed to ensure asymptotically stability in the face of model uncertainty and actuator saturation – both typical in marine applications. It also employs a real-time, in-the-loop numerical optimization algorithm to exploit the redundancy inherent in overactuated systems.

We consider the overactuated vessel to be a simplified model of our long term vision of a swarm of autonomous tugboats manipulating a disabled vessel (ex. *U.S.S. Cole*), transporting components of large offshore structures (ex. oil platforms), or positioning littoral protection equipment (ex. hydrophone arrays). Manipulation by autonomous ground vehicles has been examined before in the context of single robots or small groups of two to three robots (Lynch, 1999; Rus, 1997; Sugar and Kumar, 2002; Stilwell and Bay, 1994). However for manipulation by groups of arbitrary sizes only two methods exist: behavior based-approaches (Song and Kumar, 2002; Parker et al., 2005; Ijspeert et al., 2001; Kube and Bonabeau, 2000) which lack performance guarantees; and "kinematic caging" (Sudsang and Ponce, 2005; Wang et al., 2003; Pereira et al., 2004) which ignore second order forces and actuator saturation. Purely kinematic approaches are not suitable for marine systems. In contrast the approach presented here addresses dynamic effects and is provably correct.

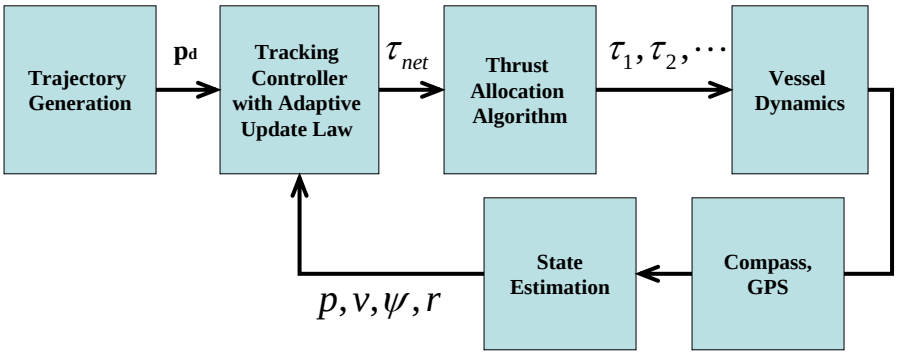

Figure 1: Our trajectory tracking framework.

The remainder of the paper is organized as follows. Section 2 reviews related work. Section 3, provides the second order dynamic model of the marine vessel and formalizes the problem statement. Section 4 presents the components of the framework: high level tracking control, adaptive parameter update, force allocation and trajectory generation. Section 5 contains simulation results, small-scale and open-water experimental results. Section 6 summarizes our contributions and discusses future work.

2 Overview, Contributions and Related Work

Overactuated and fully actuated tracking control in a marine setting has been considered before, but almost exclusively in the context of large vessels with "thruster pods" such as commercial cruise ships, for examples see (Fossen, 2002), (Johansen et al., 2004), (Pettersen et al., 2004), or (Webster and Sousa, 1999). In such works, the systems are typically only moderately overactuated (Arrichiello et al., 2009) and/or the actuator configuration has some specialized structure that can be exploited (e.g. differential thrust, dual rudder, unconstrained forces, etc.). Such approaches can be inextensible to systems with arbitrary actuator configurations. Most importantly, many of those works assume the model parameters are known exactly. In contrast, our framework (Figure 1) accounts for actuator saturation, model uncertainty and is applicable to arbitrary thruster configurations. It consists of four aspects: (1) Grasp Planning; (2) High Level Tracking Control; (3) Thrust Allocation; and (4) Trajectory Generation.

Grasp Planning: Consider the idealized schematic of a set of thrusters (representing tug boats) attached to a barge in Figure 2. The configuration of the thrusters is related to planning the grasp of a robot hand (Murray et al., 1994). It can be optimized, as in our companion work (Esposito, 2008). Works such as (Sorensen et al., 1997) consider thruster interaction and propeller wash as well. However in this paper such issues are not considered; it is merely assumed the thruster configuration renders the system overactuated and fully controllable, and that their configuration is static.

High Level Tracking Controller: Assuming the ship is fully actuated, a standard tracking controller, similar to (Loria et al., 2000; Fossen et al., 2001; Lindegaard and Fossen, 2003; Pettersen et al., 2004), is used to generate the desired, idealized net control force and moment τ_{net}. We incorporate adaptive terms which account for uncertainties in the hydrodynamic coefficients. Adaptive control for other Euler-Lagrange systems has been considered in (Spong et al., 2006; Khalil, 2001) and specifically (Fossen and Paulsen, 1992; Loria et al., 2000; Skjetne et al., 2004). The primary contribution of this paper is the construction of the adaptive components so as to retain asymptotic stability in the face of actuator saturation.

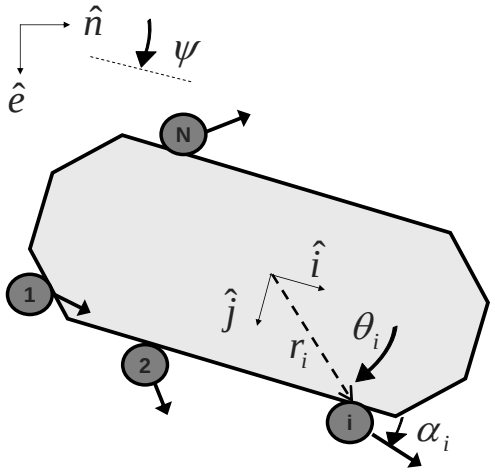

Figure 2: Overactuated Manipulation Scenario. N thrusters, representing tug boats, (dark circles) are attached to the object (shaded polygon); and can apply forces at some fixed incident angles. The position of the i^{th} thruster is defined by the angle θ_i and the push direction by the angle α_i.

Thrust Allocation: Given the desired net force and moment τ_{net}, actuator redundancy and constraints must be resolved in real time to implement the command on the N individual actuators $\tau_1, \tau_2, \ldots, \tau_N$. This approach has been tested on both scale model (Berge and Fossen, 1997) and large scale ships before (Sordalen, 1997). Some methods exploit special structure of actuators (Bordignon and Durham, 1995; Lindegaard and Fossen, 2003). Most generalizable approaches use numerical optimization methods such as sequential quadratic programming (Webster and Sousa, 1999), (Johansen et al., 2004). Our primary contribution is to cast the problem as a constrained least squares problem, similar to (Harkegard, 2002), and apply a barrier method (Boyd and Vandenberghe, 2004) which is guaranteed to solve extremely large problems in realtime as part of the control loop.

Trajectory Generation: We generate trajectories with a simple bang-bang acceleration profile (Fossen, 2002; Spong et al., 2006) to move the ship to a desired position and orientation. The novel component of the algorithm presented here is that actuator configuration and constraints, model uncertainty and controller structure are all accounted for to generate a feasible trajectory that the controller can track.

In summary, the major contribution of this paper is that each facet of the frame work is constructed to ensure asymptotically stability in the face of model uncertainty and actuator saturation – both typical in a marine applications. In addition, the thrust allocation method is extensible to arbitrary actuator configurations and accounts for unidirectional force constraints. Such constraints can model scenarios in which robots rely on friction to maintain contact with the object being manipulated; or actuator designs that are extremely inefficient when run in reverse. Finally, in addition to simulation and tank testing, this paper includes experimental validation of the tracking controller in open-water – subject to wind, waves and position sensing errors.

3 System Model

We refer to the object to be manipulated, as a *barge*. Mathematically, it is defined by a compact, convex set $\mathcal{O} \subset \mathbb{R}^2$. We assume the thrusters are rigidly attached. In the extension to swarms, this would be equivalent to the tugboats having arrived at their desired contact positions around the perimeter of the barge and mooring to its hull. Collectively we refer to the structure as the tug-barge assembly, or simply the *assembly*. Define a body-fixed coordinate frame $(\hat{i}, \hat{j}, \hat{k})$ attached to the centroid of the assembly (see Figure 2) such

that $\hat{i}$ points along the nominal forward direction, $\hat{k}$ points down and $\hat{j}$ is defined according to the right hand rule. Define the inertial coordinate system $(\hat{n}, \hat{e}, \hat{d})$ fixed at some convenient local reference point and oriented according to the North, East Down convention.

Assumption 1 *Heave (vertical), pitch and roll motions are negligible.*

Therefore, we employ a planar 3-DOF, second-order dynamic model (Fossen, 2002)

$$\dot{p} = R(\psi)\nu \quad (1)$$

$$M\dot{\nu} + C(\nu)\nu + D(\nu) = \tau_{net} = B\tau, \quad (2)$$

where the position and yaw angle of barge are described in the inertial frame as $p = [x, y, \psi]^T$. It is more convenient to express the barge's velocity in the body frame $\nu = [u, v, r]^T$ (also called surge, sway and yaw rate). $R(\psi)$ denotes the rotation matrix from the body frame to the inertial frame and is defined as

$$R(\psi) = \begin{bmatrix} \cos(\psi) & -\sin(\psi) & 0 \\ \sin(\psi) & \cos(\psi) & 0 \\ 0 & 0 & 1 \end{bmatrix}. \quad (3)$$

M represents the effective mass/inertia matrix of the assembly defined in the body frame, including added mass (Fossen, 2002); and $D(\nu)$ represents the hydrodynamic drag forces on the assembly, defined in the body frame. $C(\nu)$ represents the Coriolis-centripetal matrix. These terms are discussed in more detail later.

The right hand side of (2) is the net applied force/moment on the barge, $\tau_{net} = [F_u, F_v, M_r]^T$, due to the N thrusters (tugboats). $\tau = [\tau_1, \dots \tau_N]^T \in \mathcal{T} \subset \mathbb{R}^N$ is a vector of input thrust *magnitudes* for each tugboat. Most tugboats have propellers and engines that are significantly less efficient when run in reverse; and have upper limits on the thrust that they can apply – very often two or more tugs are required to generate enough force to move the barge. This motivates the following assumption.

Assumption 2 *The set of feasible thruster magnitudes, $\mathcal{T}$, can be described as $0 \leq \tau_i \leq \tau_{\max}, \forall i \in [1, \dots, N]$.*

Finally $B \in \mathbb{R}^{3\times N}$ captures the geometric configuration of the thrusters (tugs) relative to the body frame of the barge and requires additional notation to define (see Fig. 2). The barge boundary is denoted by $\partial\mathcal{O}$. Assuming it is convex allows us to parameterize the points on the boundary in polar coordinates using the angle θ, measured clockwise, relative to the $\hat{i}$ axis of the body frame and distance to the center of gravity r. The position of the i-th thruster is

$$\{r_i \cos\theta_i \hat{i} + r_i \sin\theta_i \hat{j} \in \partial\mathcal{O}, \forall\theta \in \mathbb{S}^1\}. \quad (4)$$

In addition, define the angle $\alpha \in \mathbb{S}^1$ which indicates the direction of the push force, measured clockwise relative to the $\hat{i}$-axis of the body frame. The i^{th} column of the thruster configuration matrix is

$$B_i = \begin{bmatrix} \cos\alpha_i \\ \sin\alpha_i \\ -r_i \sin\theta_i \cos\alpha_i + r_i \cos\theta_i \sin\alpha_i \end{bmatrix}. \quad (5)$$

Note that we do not constrain the possible push directions, α_i, but do consider them fixed. Therefore:

Assumption 3 *The thruster configuration matrix B is time invariant in the body frame.*

Finally, synthesizing the optimal placement of the tugs is beyond the scope of this paper (Esposito, 2008); however it is possible that a completely arbitrary thruster configuration may not render the assembly small time locally controllable, especially under the unidirectional actuator constraints.

Assumption 4 *The columns of the B matrix positively span $\mathbb{R}^3$, ensuring the system is controllable and fully actuated.*

This condition is related to the concept of force closure in the robotic grasping literature, and is easily tested (Murray et al., 1994). It is well known that at least 4 thrusters are required to satisfy this condition.

Returning to the matrices M, C, and D.

Assumption 5 *We assume the assembly possesses port-starboard symmetry; the centers of gravity, added mass and drag coincide; and the assembly rotates at moderate speeds.*

Therefore

$$M = \begin{bmatrix} m_u & 0 & 0 \\ 0 & m_v & m_{rv} \\ 0 & m_{rv} & I_r \end{bmatrix} \tag{6}$$

where m is the effective mass, including added mass, in the various directions, and I_r is the rotational moment of inertia about the yaw axis ($\hat{k}$).

$$C(\nu) = \begin{bmatrix} 0 & 0 & -m_v v - m_{rv} r \\ 0 & 0 & m_u u \\ m_v v + m_{rv} r & -m_u u & 0 \end{bmatrix}. \tag{7}$$

We use a linear-quadratic drag model $D(\nu) = D_l \nu + D_n(\nu)\nu$, where

$$D_l = \begin{bmatrix} X_u & 0 & 0 \\ 0 & Y_v & Y_r \\ 0 & N_v & N_r \end{bmatrix} \tag{8}$$

and

$$D_n(\nu) = \begin{bmatrix} X_{uu}|u| & 0 & 0 \\ 0 & Y_{vv}|v| & Y_{vr}|v| \\ 0 & N_{vv}|v| & N_{vr}|v| \end{bmatrix} \tag{9}$$

with $|u|$ or $|v|$ indicating the absolute value (Blanke, 1981). Note that our tank testing (Fig. 14) empirically justifies the drag model.

4 Approach

Our approach was developed to yield stable trajectory tracking in the face of actuator limits and uncertain hydrodynamic parameters. It is divided into four parts: tracking controller design, uncertainty management, thrust allocation and trajectory generation. Each component must be carefully designed to yield overall system stability.

4.1 Tracking Control

Problem 4.1 *Given, the nominal ship model from (1) and (2), a twice differentiable reference trajectory $p_d(t)$, and measurements of p and ν; determine a high-level feedback law $T : \mathbb{R}^3 \to \tau_{net}$ such that $\|p_d(t) - p(t)\| \to 0$ as $t \to \infty$.*

Position and velocity tracking error signals are defined in the body frame

$$e_p = R^T(\psi)\left(p_d - p\right), \quad e_\nu = \nu - R^T(\psi)\dot{p}_d. \tag{10}$$

Then the open-loop, tracking error dynamics (Smith et al., 2007; Feemster et al., 2008) are

$$\begin{aligned} \dot{e}_p &= -S(r)e_p + e_\nu \\ \dot{e}_\nu &= \dot{\nu} + S(r)R^T(\psi)\dot{p}_d - R^T(\psi)\ddot{p}_d, \end{aligned} \tag{11}$$

where the skew-symmetric matrix $S(r)$ is defined as

$$S(r) = \begin{bmatrix} 0 & -r & 0 \\ r & 0 & 0 \\ 0 & 0 & 0 \end{bmatrix}. \tag{12}$$

The filtered tracking error $e(t) \in \mathbb{R}^3$ is defined as

$$e(t) = e_\nu + k_p e_p, \tag{13}$$

where $k_p \in \mathbb{R}^+$ denotes a positive, scalar control gain. In order to design the control input τ_{net}, it is insightful to write the open-loop filtered tracking error dynamics

$$\begin{aligned} M\dot{e} &= [-C(\nu)\nu - D(\nu) + \tau_{net}] + M\left[S(r)\left(R^T(\psi)\dot{p}_d \right.\right. \\ &\quad \left.\left. -k_p e_p\right) - R^T(\psi)\ddot{p}_d + k_p e_\nu\right]. \end{aligned} \tag{14}$$

Proposition 4.2 *Based on the open-loop tracking error dynamics (14), the vessel control input*

$$\begin{aligned} \tau_{net} &= C(\nu)\nu + D(\nu) - M\left[S(r)\left(R^T(\psi)\dot{p}_d - k_p e_p\right)\right. \\ &\quad \left. -R^T(\psi)\ddot{p}_d + k_p e_\nu\right] - e_p - ke, \end{aligned} \tag{15}$$

where $k \in \mathbb{R}^+$ is a control gain, solves the tracking problem.

Proof: After substituting the proposed control vector (15) for τ_{net} in the open-loop dynamics (14), the closed-loop dynamics of $e(t)$ become

$$M\dot{e} = -e_p - ke. \tag{16}$$

Stability and the position tracking result can be illustrated through Lyapunov analysis by defining a non-negative scalar function

$$W(t) = \tfrac{1}{2}e_p^T e_p + \tfrac{1}{2}e^T M e. \tag{17}$$

After taking the time derivative of (17) and substituting in the expressions of (11) and (16), the time derivative for $W(t)$ can be upper-bounded by

$$\dot{W} \leq -kk_p\|e_p\|^2 - k\|e\|^2, \tag{18}$$

where the fact that $e_\nu = e - k_p e_p$ has been utilized. Barbalat's Lemma (Khalil, 2001) can now be applied to (18) to illustrate asymptotic position tracking in the sense that $\lim_{t\to\infty} e_p(t), e(t) = 0$.

Remark 4.3 *It is tempting to suggest that (16) can be used to design k and k_p to obtain a desired transient response. However, as discussed in the following section, the uncertainly in the drag coefficients precludes this approach.*

4.2 Uncertainty Management

The Tracking Controller in Sect. 4.1 uses information about the barge dynamics (1),(2) to exactly cancel terms in the error dynamics (10). However in practice it is difficult to measure the drag parameters precisely. Instead, assume we only have access to imperfect estimates of the drag parameters

$$\hat{d}(t) = \left[\hat{X_u},\ \hat{Y_v},\ \hat{Y_r},\ \hat{N_v},\ \hat{N_r},\ \hat{X_{uu}},\ \hat{Y_{vv}},\ \hat{Y_{vr}},\ \hat{N_{vv}},\ \hat{N_{vr}}\right]^T$$

and we update the estimate according to

$$\dot{\hat{d}} = \begin{cases} 0 & \text{if } \hat{d} = \bar{d}, -V^T e > 0 \\ 0 & \text{if } \hat{d} = 0, -V^T e < 0 \\ -V^T e & \text{otherwise} \end{cases} \tag{19}$$

where the regressor matrix is defined as

$$V = \begin{bmatrix} u & 0 & 0 & 0 & 0 & |u|u & 0 & 0 & 0 & 0 \\ 0 & v & r & 0 & 0 & 0 & |v|v & |v|r & 0 & 0 \\ 0 & 0 & 0 & v & r & 0 & 0 & 0 & |v|v & |v|r \end{bmatrix}$$

and $\bar{d}$ denotes an *a priori* upper-bound on the values for the drag coefficients (assumed known). Note that the derivative is "projected" to zero at the extremes of the interval $[0, \bar{d}]$. These bounds reflect the physics of the problem and will be used later to insure the control law respects the actuator limitations.

Proposition 4.4 *If the control law from (15) is replaced with*

$$\begin{aligned} \tau_{net} = \; & C(\nu)\nu + V\hat{d} - M\left[S(r)\left(R^T(\psi)\dot{p}_d - k_p e_p\right)\right. \\ & \left. -R^T(\psi)\ddot{p}_d + k_p e_\nu\right] - e_p - ke \end{aligned} \tag{20}$$

and $\hat{d}$ is updated according to the adaptive update law in (19), the control law causes $e(t) \to 0$ even if $\hat{d}(0) \neq d$.

Proof: Define the parameter estimate error as

$$\tilde{d} = d - \hat{d}. \tag{21}$$

Consider the Proof in Sect. 4.1. The closed loop error dynamics (16) become

$$M\dot{e} = -V\tilde{d} - e_p - ke. \tag{22}$$

Define a new scalar function

$$W = \tfrac{1}{2} e_p^T e_p + \tfrac{1}{2}\tilde{d}^T\tilde{d} + \tfrac{1}{2} e^T M e. \tag{23}$$

Taking the time derivative and substituting (11) and (19) leaves the upper bound on $\dot{W}$ in (18) unchanged–implying that $\lim_{t\to\infty} e_p(t), e(t) = 0$.

4.3 Thrust Allocation Strategy

With the design of $\tau_{net}(t)$ complete, the subsequent task is to now specify the individual thruster commands such that their combined effort approximates $\tau_{net}(t)$ as closely as possible. Therefore, the thrust allocation strategy must solve the following linearly constrained least squares problem.

Problem 4.5 *Given a desired τ_{net} from (20), determine $\tau \in \mathbb{R}^N$ according to*

$$\min_{\tau} \|B\tau - \tau_{net}\|^2 \tag{24}$$

such that

$$0 \leq \tau_i \leq \tau_{\max}, \;\; i = 1, \ldots, N. \tag{25}$$

Remark 4.6 *The linearly constrained least squares problem is known to be convex, therefore it returns a globally optimal solution. Therefore, provided τ_{net} is consistent with the actuator limitations, $B\tau = \tau_{net}$.*

Remark 4.7 *Such convex optimization problems can be solved using a barrier method in real time, as part of the feedback loop; and scale well, $O(N^2)$, with the number of thrusters (Boyd and Vandenberghe, 2004).*

4.4 Trajectory Generation

As noted above, the Thrust Allocation Strategy is only guaranteed to properly realize τ_{net} if it is consistent with the actuator limitations. Likewise, our proof for controller stability does not explicitly account for actuator limitations. A critical component of our control strategy is to generate desired trajectories that do not saturate the actuators. We discuss this further in the Remarks following the algorithm presentation.

Problem 4.8 *Given the mass M, upper bounds on the drag coefficients $\bar{d}$, the actuator limit $\tau_{\max}$, and initial and final desired positions, p_d^0 and p_d^f, find $p_d(t)$ such that*

- *$p_d(0) = p_d^0$, $p_d(t_f) = p_d^f$, where t_f is an unspecified final time; and*
- *$\tau \in \mathcal{T}$ during steady state tracking.*

Our approach is presented in Algorithm 1. We first compute an upper bound on the realizable τ_{net} for a given thruster configuration B. We then use the structure of the tracking controller to place constraints on the trajectory, p_d, and its derivatives. Finally, we generate bang-bang trajectories that comply with those bounds. The details are explained below.

Algorithm 1 : Generate Trajectory $(M, \bar{D}, B, \tau_{\max}, p_d^0, p_d^f) \rightarrow (a_x, a_y, a_\psi, t_s)$

```
Determine τ̄_net using (26)
Solve for a_tran, a_ψ using (30)
Solve for t_s^tran and t_s^ψ using (31)
if t_s^tran > t_s^ψ then
   t_s = t_s^tran
   Rescale a_ψ using (32)
else
   t_s = t_s^ψ
   Rescale a_tran using (33)
end if
Resolve a_tran into components a_x and a_y
```

First, given the B matrix and the actuator bounds $\tau_i \in [0, \tau_{\max}]$, it is possible to compute an isotropic, conservative, upper-bound on τ_{net}, by searching for the direction in which τ_{net} is weakest when all the inputs are set to $\tau_{\max}$ (Esposito, 2008) using

$$\bar{\tau}_{net}(B, \tau_{\max}) = \min_{j,k \in N \times N} \tau_{\max} \sum_{i=1}^{N} \max(0, \frac{B_j \times B_k}{\|B_j \times B_k\|} \cdot B_i). \tag{26}$$

Regarding the τ_{net} generated by the control law (20), after some initial transient the error signals go to zero leaving the following terms,

$$\tau_{net} \approx M\left(R^T \ddot{p}_d + S(\dot{\psi}_d) R^T \dot{p}_d\right) + \tag{27}$$

$$V(R^T \dot{p}_d)\bar{d} + C(R^T \dot{p}_d) R^T \dot{p}_d. \tag{28}$$

Next, we elected to consider straight line bang-bang trajectories of the form:

$$\ddot{p}_d = \begin{cases} [a_x, a_y, a_\psi]^T, & 0 < t \leq t_s \\ [-a_x, -a_y, -a_\psi]^T, & t_s < t \leq 2t_s \end{cases} \tag{29}$$

where a_x, a_y, and a_ψ are constant accelerations defined in the inertial frame and t_s is the switching time which is unspecified but, by symmetry, half the final time (Spong et al., 2006).

In order to find $a = [a_x, a_y, a_\psi]^T$ such that $\tau_{net} \leq \bar{\tau}_{net}$, it is convenient to define $a_{tran} = \|[a_x, a_y]\|$, $d_{tran} = \|[x_f - x_0,\ y_f - y_0]\|$ and $d_\psi = \psi_f - \psi_0$ such that $-\pi < d_\psi \leq \pi$. From the form of the bang-bang trajectory, the peak acceleration is a and peak magnitude of the translational and rotational velocity signals are $\sqrt{d_{tran} a_{tran}}$ and $\sqrt{d_\psi a_\psi}$ respectively, which occur at $t = t_s$. Finally, we make the following conservative assumption. The worst case trajectory would be such that $\ddot{p}_d$ and $\dot{p}_d$ are directed along the body axis with the largest mass and drag parameters respectively (typically the $\hat{j}$ axis). Therefore by substituting into (27), if we solve the following nonlinear equation for a_{tran} and a_ψ

$$\begin{aligned} \Big(\max(m_u, m_v)(a_{tran} + \sqrt{d_{tran} a_{tran}}\sqrt{d_\psi a_\psi}) \\ + \max(\bar{X}_u, \bar{Y}_v)\sqrt{d_{tran} a_{tran}}\Big)^2 + \\ (I_r a_\psi + N_r \sqrt{d_\psi a_\psi})^2 = (\bar{\tau}_{net})^2 \end{aligned} \tag{30}$$

we can generate a trajectory which respects the actuator limitations. A numerical non-linear equation solver is employed for this computation, computational cost is addressed in Sect. 5.2.

From the accelerations we can determine the switching times required to arrive at the halfway point are

$$\begin{aligned} t_s^{tran} &= \sqrt{d_{tran}/a_{tran}}, \\ t_s^{\psi} &= \sqrt{d_\psi/a_\psi}. \end{aligned} \tag{31}$$

By symmetry the final times are twice the switching times. We use the larger of the two as the actual switching time $t_s = \max(t_s^{tran}, t_s^{\psi})$ and re-scale the acceleration corresponding to the smaller switching time using

$$a_\psi = d_\psi / t_s^2 \tag{32}$$

$$a_{tran} = d_{tran} / t_s^2 \tag{33}$$

as appropriate. Finally a_{tran} can be separated into components a_x and a_y in the inertial frame.

Remark 4.9 *One of our primary objectives is to avoid actuator saturation. In the absence of external disturbances we achieve this because:*

1. *We have selected our peak desired acceleration and trajectory duration by explicitly considering $\tau_{\max}$.*
2. *Also, we generate our trajectory such that $p_d(0) = p(0)$ (from GPS), and $\dot{p}_d(0) = \dot{p}(0) = 0$. Therefore the error signals are initially zero, $e_p(0) = 0$ and $e_\nu(0) = 0$ – precluding any saturation during the initial transient.*

Finally, it should be said that in the field, with wind and waves present, it is impossible to guaranteed the actuators are not saturated. It can happen that, for example, the drag from gale force winds could overpower the actuators – preventing the errors from converging to zero. This is a practical limitation of any actuator with finite energy. In light winds it is possible to mitigate this effect by using "safety factor" when generating the trajectory – e.g. $\tau'_{\max} = 0.9\tau_{\max}$.

Remark 4.10 *Note that the trajectory is not truly time optimal for two reasons. First (26) and (30) introduce some conservatism. Second by assuming the trajectories are of the straight line, bang-bang class in both translation and rotational components, we preclude solutions that exploit the fact that the barge has a preferential motion direction that is more efficient for executing large translations (typically along the $\hat{\imath}$-axis).*

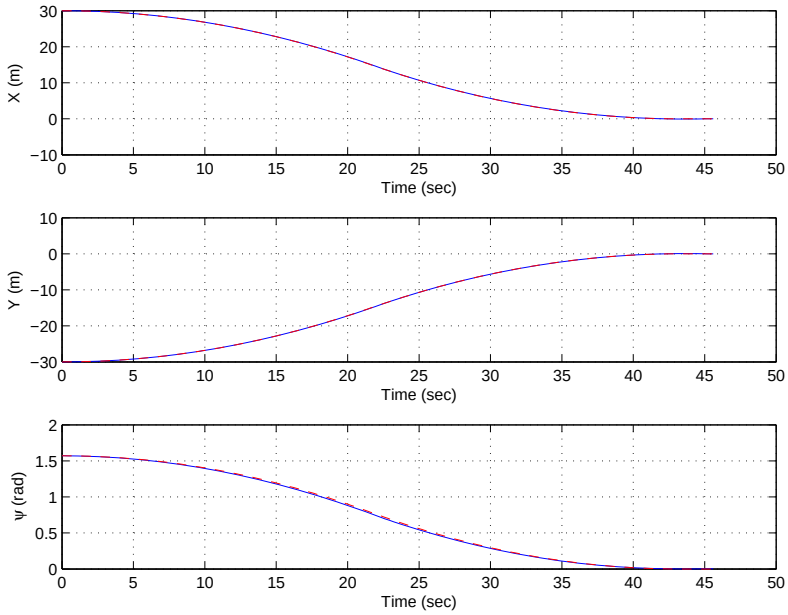

Figure 3: Desired position, p_d (solid) and simulated position, p (dashed) vs. time.

5 Results

5.1 Simulation Study

The approach described in Section 4 was simulated using MATLAB SIMULINK. The hydrodynamic parameter values from (Pettersen et al., 2004) were used

$$\begin{aligned} M &= \text{diag}\{\ 19.0\ (kg),\quad 35.2\ (kg),\quad 4.2\ (kg \cdot m^2)\ \} \\ D &= \text{diag}\{\ 4.0\ (\tfrac{N\,\text{sec}}{m}),\quad 10.0\ (\tfrac{N\,\text{sec}}{m}),\quad 1.0\ (Nm \cdot \text{sec})\ \}. \end{aligned}$$

The maximum thrust value was $\tau_{\max} = 25N$. The swarm configuration about the barge hull was selected as

$$\begin{array}{lll} \alpha_1 = 10^\circ, & r_1 = 1.4\ (m), & \theta_1 = 190^\circ \\ \alpha_2 = 75^\circ, & r_2 = 0.87\ (m), & \theta_2 = 205^\circ \\ \alpha_3 = 100^\circ, & r_3 = 0.57\ (m), & \theta_3 = 275^\circ \\ \alpha_4 = 180^\circ, & r_4 = 1.7\ (m), & \theta_4 = 17^\circ \\ \alpha_5 = 250^\circ, & r_5 = 0.87\ (m), & \theta_5 = 125^\circ \\ \alpha_6 = 272^\circ, & r_6 = 0.57\ (m), & \theta_6 = 94^\circ. \end{array} \tag{34}$$

Figure 3 depicts $p_d(t)$ computed by the trajectory generator. The accelerations are $a = [-0.0641, 0.0641, -0.0034]$ and the switch time is $t_s = 21.63$ sec. Regarding the tracking controller, the gains $k_e = 1.0$ and $k_p = 5.0$ were used. Again Figure 3 shows the actual inertial positions p compared to p_d. Figure 4 shows the error signals decaying to zero – never exceeding 3 cm. The error peaks at the switching time when the acceleration changes abruptly. Note the time scale is extended in this figure to show the errors decay to zero at steady state.

Note that in this configuration, with $\tau_{\max} = 25$, the net force limit is $\bar{\tau}_{net} = 52.3\ (N)$ according to (26). The trajectory generator selected a to keep $\tau_{net} \leq \bar{\tau}_{net}$, this property is apparent in Figure 5. With regard to the force allocation method, Figure 7 depicts the individual thrust values. Note that $0 \leq \tau_i \leq \tau_{\max}$ at all times. Also, the τ_{net} generated by the optimization routine was generally within $\pm 2\ N$ (Nm resp.) of the desired τ_{net} as seen in Fig. 6 and the numerical algorithm converged in a mean runtime of 0.01 sec on a

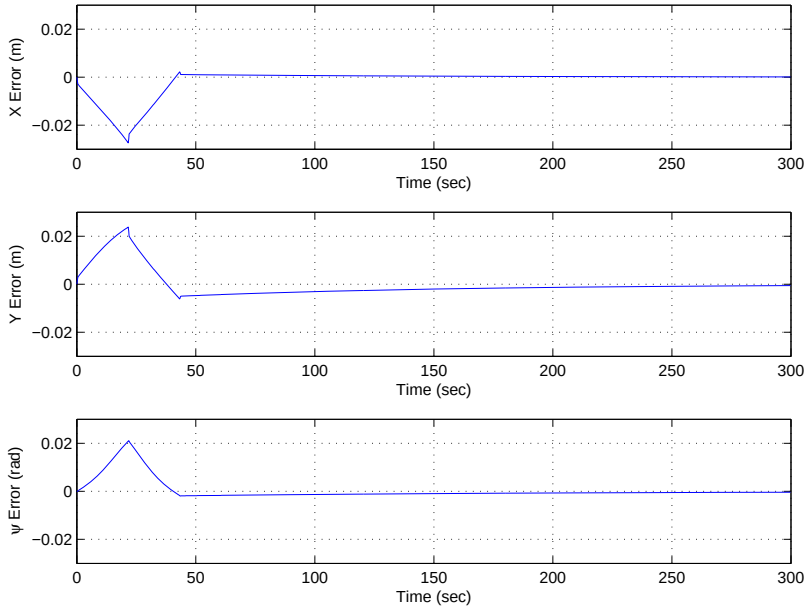

Figure 4: Tracking Error $e_p = p_d - p$ vs. time. Note the extended time scale used to illustrate steady state convergence.

1 Ghz Laptop. The geometry of the actuators implies that at a global optimum of the objective function, tugs 1 (forward)and 4 (reverse) should never be on simultaneously (also 2 and 5; and 3 and 6). This can be verified in Fig. 7.

Finally, Figure 8 illustrates the evolution of our uncertain drag coefficient estimate $\hat{d}$. Note that there is no guarantee that $\hat{d}$ converges to the true value of d, without the persistent excitation criteria (Khalil, 2001). Our adaptive law is simply selected to promote asymptotic tracking – not parameter identification.

5.2 Small Scale Experiments

As a first step to experimental validation, without having to worry about external disturbances such as wind, waves, current and Global Positioning System (GPS) errors, a small scale experimental vessel was constructed (Fig. 9). The vessel is designed for indoor operation inside the United States Naval Academy's 100.0 meter tow tank facility. Figure 10 illustrates the actuator configuration used, detailed below.

$$\begin{array}{lll} \alpha_1 = 0^\circ, & r_1 = 1.346\ (m), & \theta_1 = 180^\circ \\ \alpha_2 = 90^\circ, & r_2 = 0.873\ (m), & \theta_2 = 225^\circ \\ \alpha_3 = 90^\circ, & r_3 = 0.571\ (m), & \theta_3 = 270^\circ \\ \alpha_4 = 180^\circ, & r_4 = 1.702\ (m), & \theta_4 = 0^\circ \\ \alpha_5 = 250^\circ, & r_5 = 0.873\ (m), & \theta_5 = 135^\circ \\ \alpha_6 = 270^\circ, & r_6 = 0.571\ (m), & \theta_6 = 90^\circ \end{array} \tag{35}$$

The hull of the "barge" is a $1/36^{th}$ scale model of a U.S. Navy Yard Patrol Craft. It measures approximately 1.0 m in length and 0.3 m wide. Six marine bilge pumps were attached to the vessel to act as our swarm of tug boats. Each bilge pump is powered by a 12.0 V, H-bridge power amplifier, the mechanical design of the pumps is such that they can only produce thrust in one direction. The maximum value of a single pump's thrust is approximately 5 (N). Since the experiment was conducted indoors, standard global positioning sensors could not be employed to provide the inertial position signals. Instead, a digital video camera was mounted above the workspace and interfaced a shore-based laptop running MATLAB's Image Acquisition

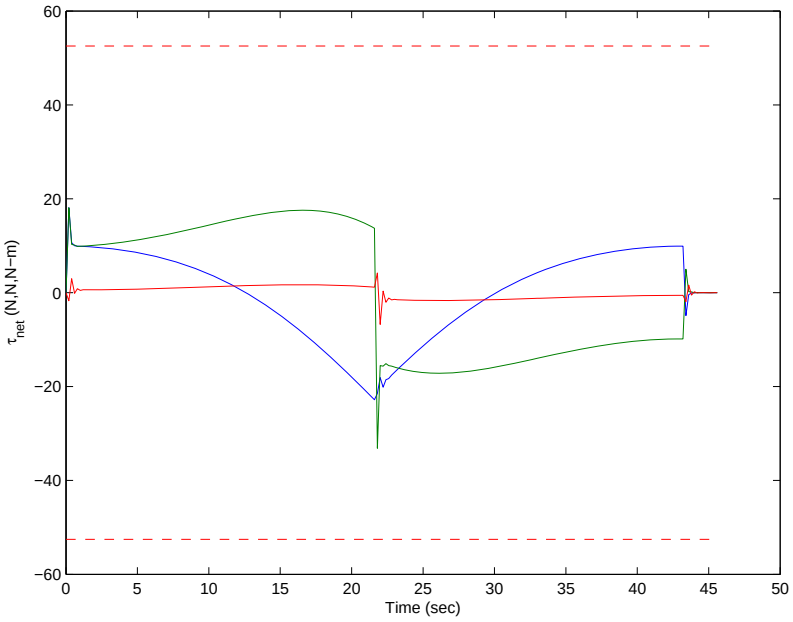

Figure 5: Net Force/Moment vs. Time. (Blue) F_x, (Green) F_y, and (Red) M_z. Dashed lines indicate bounds on net force/torque.

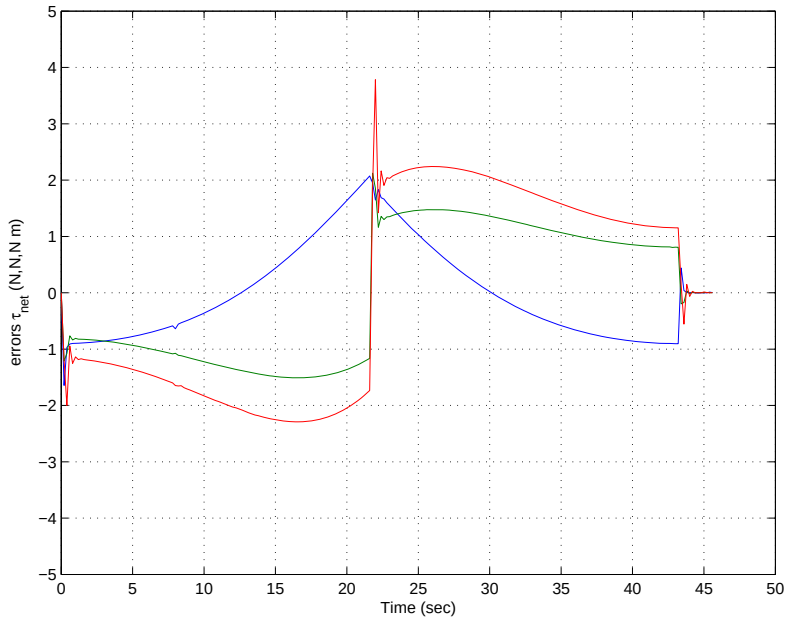

Figure 6: Error of Force Allocation Algorithm vs. Time. (Blue) F_x, (Green) F_y, and (Red) M_z.

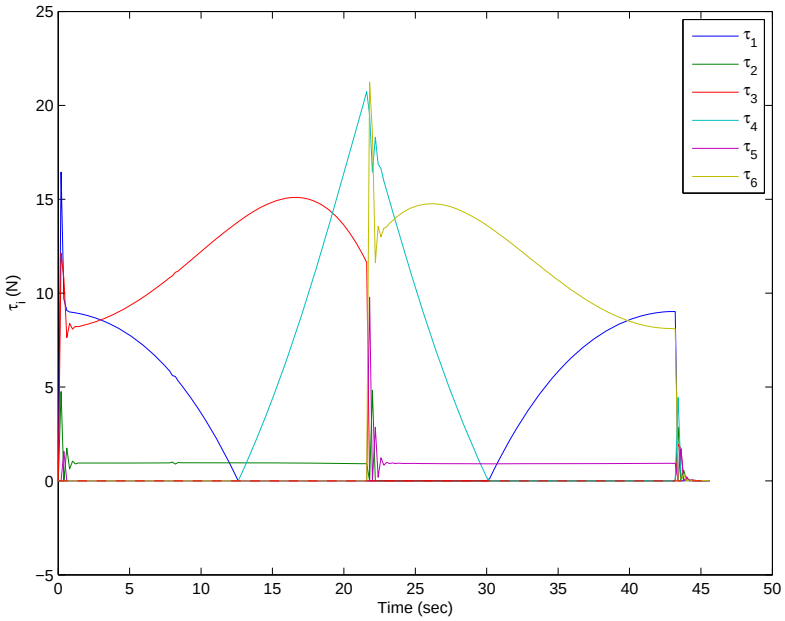

Figure 7: Thrusts vs. Time.

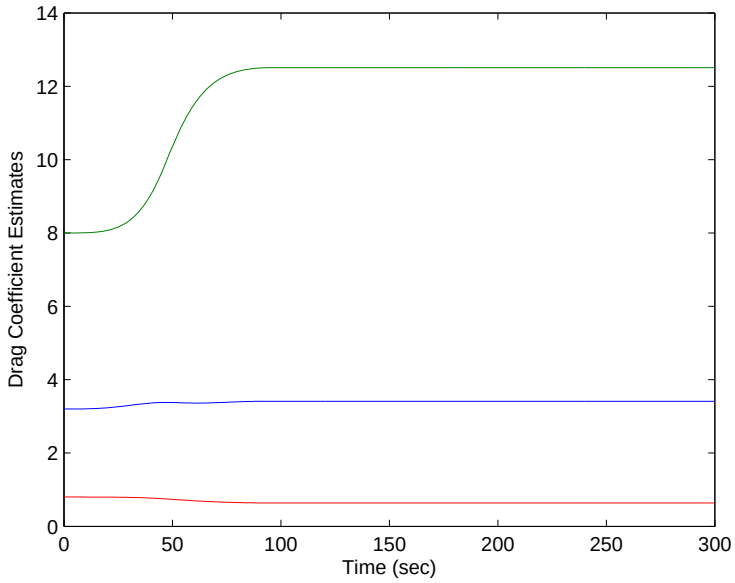

Figure 8: Drag Parameter Estimates, $\hat{d}$ vs. Time. (Blue) d_u, (Green) d_v, and (Red) d_r.

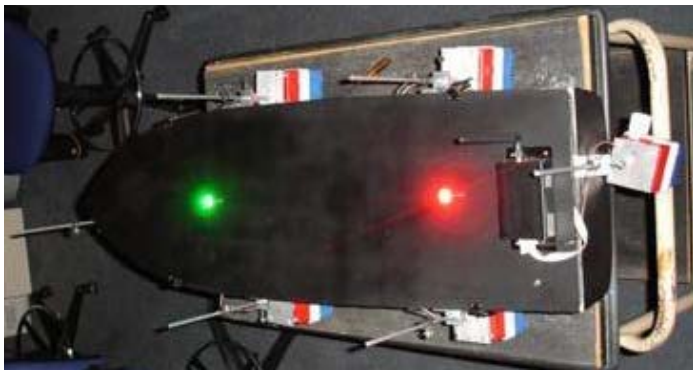

Figure 9: Small-scale indoor experimental apparatus (overhead view).

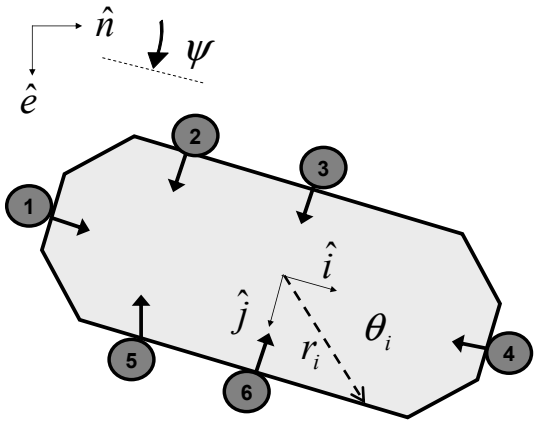

Figure 10: Actuator geometry for both the indoor and open water experiments.

Toolbox. Two high intensity LEDs mounted on top of the vehicle provide active color features (see Fig. 9) from which the (x, y) position and heading, ψ, of the vessel is determined. The laptop is equipped with a MaxStream Wireless RS232 modem. After it processes the image, it broadcasts position readings to the ship-board microprocessor.

There are two important issues regarding this position measurement set up: update frequency and accuracy. Regarding frequency, the camera was configured to to acquire video at 10 frames per second. This frame rate was justified in two ways. First, simulation experiments suggested updates should be more frequent than 5 Hz to ensure stability for the indoor set up. This is primarily due to the lower drag coefficients and shorter travel distances (relative to hull length), as compared with the outdoor set up which may get GPS updates as infrequently as 0.5 HZ. Second, initial testing indicated that the image acquisition, processing, wireless transmission and control law computation took between 0.05 and 0.067 sec. Therefore we were highly confident that the entire loop could be reliably closed in 0.1 sec. *Post hoc* analysis confirmed this to be true. The active color features, combined with the uniform darkness of the boat deck and low ambient light levels inside the tow tank, facilitated efficient image processing in MATLAB. The second concern is latency. The total latency from image acquisition to control implementation was estimated to be on the order of 0.1 sec (1 frame). Obviously, latencies of up to one frame can be related can be attributed to processing time. However latencies can also arise from the acquisition process. We took the following steps to minimize latency, proper trigger configuration (camera and MATLAB setting), allowing for camera warm up, and reducing exposure time. In our experience, the exposure time has the largest influence. The camera was configured to have a fixed exposure setting (vice auto-exposure). The intensity of the active color features (1 Watt LEDs) was tested and selected intentionally to permit good acquisition in dark environment with small, fixed, exposure times.

The second issue is position estimate accuracy. The camera provides a 640×480 pixel image and was mounted approximately 7.0 meters overhead. The MATLAB Camera Calibration Toolbox developed at CalTech was used (Bouguet, 2009), along with a checkerboard-style calibration pattern placed on a floating platform, to recover the intrinsic and extrinsic parameters of the camera. Since the boat's motion evolves in a plane, actual position data can be recovered from a single image. We used Brown's radial plus tangential model (Brown, 1971) to approximate the barrel distortion induced by the camera. Our experience indicates it is only severe at the edges of the image. We deliberately chose the starting and desired location at least 20 pixels away from the image edges. By moving the calibration pattern to other locations in the image and performing corner detection we determined the root mean squared calibration error was on the order of 0.03 m. Given the distance between the features, this translates to approximately a ± 2.5 degree orientation error.

Finally, the fixed camera/laptop pose estimates were transmitted to the ship-board Rabbit processor via pair of MaxStream Wireless RS232 serial modems. The control strategy is executed using the on-board Rabbit 3000 microprocessor. The required velocity signals of $\dot{p}(t)$ were generated through a backwards difference scheme coupled with a low pass filter.

The primary purpose of these early experiments was to examine the behavior of the adaptive control strategy in a controlled environment. Therefore, the optimization routine of the force allocation strategy was replaced with a closed form solution (Braganza et al., 2007). In addition, the trajectory was a simple setpoint $p_d(t) = p_d^f$, and $\dot{p}_d(t) = \ddot{p}_d(t) = 0$. For the experiment, the following initial/final position/orientation was used:

$$\begin{array}{rcl} p(0) & = & \left[\begin{array}{ccc} 4.64\ (m), & 0.93\ (m), & 205.40^o \end{array} \right]^T, \\ p_d(t) & = & \left[\begin{array}{ccc} 2.0\ (m), & 3.0\ (m), & 180.0^o \end{array} \right]^T. \end{array} \tag{36}$$

The control gains were selected, based on simulation results, as $k_e = 0.3$, $k_p = 0.5$. The numerical values for the mass matrix were estimated to be

$$M = \text{diag}\{ \begin{array}{ccc} 15.5\ (kg), & 15.5\ (kg), & 1.5\ (kg \cdot m^2) \end{array} \}. \tag{37}$$

The exact drag coefficients are unknown. However previous hydrodynamic test data (Compton et al., 2008)

indicates, without the 6 bilge pumps attached,

$$D = \text{diag}\{\ 0.0495\ (Nsec/m),\quad 1.521\ (Nsec/m),\quad 0.112\ (Nmsec/rad)\ \}. \tag{38}$$

Therefore, the initial values for the parameter estimate vector $\hat{d}$ was selected as

$$\hat{d}(0) = \left[\ 0.05,\quad 1.5,\quad 0.15\ \right]^T. \tag{39}$$

The (x, y) position of the center of mass of the barge and heading angle ψ is illustrated in Fig. 11 with the drag parameter estimates shown in Fig. 12. From Figure 12, one can observe that the parameter estimates approach a constant value in approximately 40.0 (sec).

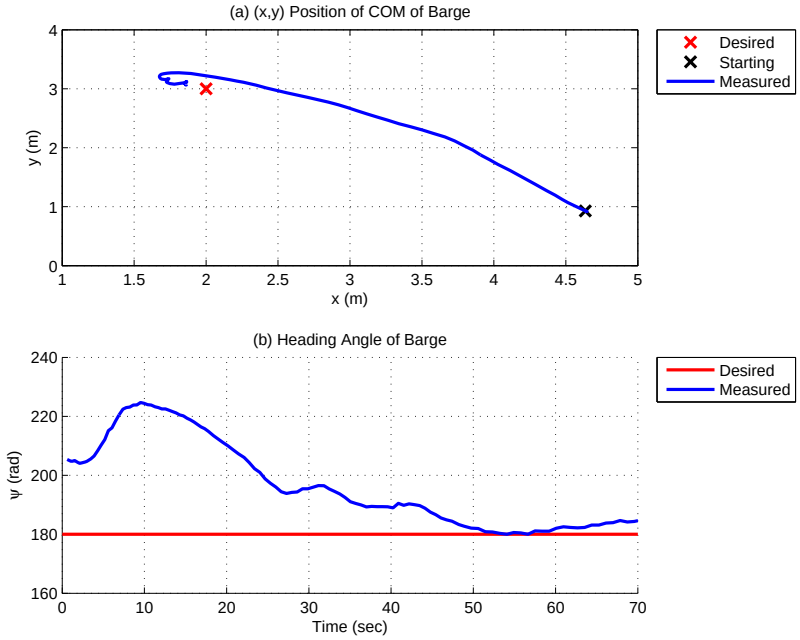

Figure 11: (a) (x, y) Barge Position (b) Heading ψ.

Remark 5.1 *It should be noted that the adaptive update law of (19) was not designed to identify the drag coefficients $D = diag\{d_u, d_v, d_r\}$; but rather, to satisfy the position/orientation tracking error objective by ensuring that the Lyapunov function $W(t)$ is negative semi-definite. However, the steady state values are slightly higher than those from scaled hydrodynamic testing (Compton et al., 2008). This is reasonable given that the addition of the 6 bilge pumps would only increase the drag coefficients, particularly in the $\hat{i}$-direction.*

5.3 Open-Water Experimental Results

In this section, we present experimental results using the full approach outlined in Section 4. Our outdoor test bed is a ten foot surface vessel (see Figure 13) outfitted with six trolling motors (Minn Kota, 133 N thrust) that represent the attached autonomous tugboats. The configuration of the trolling motors is identical to the indoor experiments, shown in Fig. 10 and detailed in (35). The assembly's mass matrix is approximated with the following values (the off diagonal terms were assumed to be zero)

$$M = \begin{bmatrix} 218\ (kg) & 0 & 0 \\ 0 & 218\ (kg) & 0 \\ 0 & 0 & 25\ (kg \cdot m^2) \end{bmatrix} \tag{40}$$

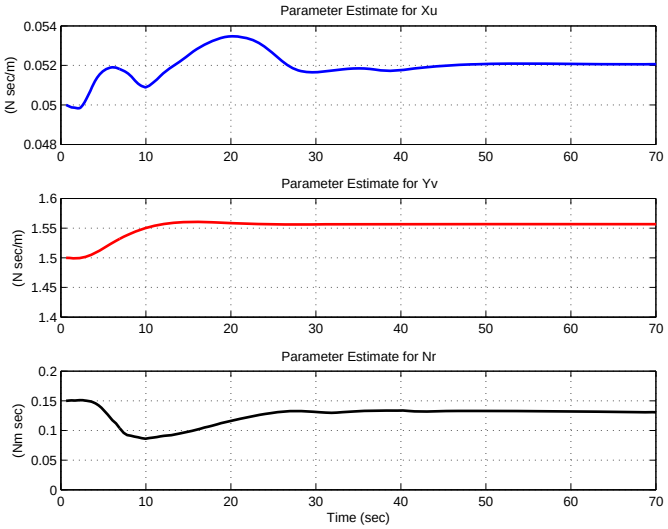

Figure 12: Parameter Estimates for Drag Effects.

To gauge the drag effects for this setup, the assembly was towed at known speeds, using an instrumented gantry, inside USNA's testing tank and the resulting forces were measured. Figure 14 displays the measured and modeled drag force in the surge direction – clearly demonstrating the quadratic drag phenomenon. Similar experiments were conducted in the sway and yaw directions.

Regarding the control implementation, the trolling motors were powered by three, dual channel RoboteQ (Model ADX3500) power amplifiers that received their duty cycle commands via serial RS232 from a Rabbit 3000 microprocessor equipped with six serial ports. A deep cycle marine battery provided the 12 (V) power bus. The position of the boat was measured with a ruggedized, weather-proof, global position sensor typically used in surveying applications (Trimble Pathfinder Pro $2,500), which reports horizontal root mean squared position accuracy to $\pm 1m$. The heading of the boat was measured with a magnetic compass (KVH Model C100 compass engine). The NMEA 0183 GPS string and the compass output were read via RS232 into a laptop running MATLAB where the high level controller of (15) was calculated. The individual tugboat thrust commands τ were calculated in soft real time via the thrust allocation approach of Section 4.3 and sent serially to the Rabbit 3000 for distribution among the trolling motors.

The vessel in Figure 13 was launched in the Mill Creek basin area – a small cove off of the larger Magothy River in Severna Park, Maryland, USA. As shown in Figure 19, it was required to start from $(38.9921135°, -76.45382535°)$, traverse to the intermediate waypoint location $(38.99205°, -76.45345°)$ and then return to its starting point. As seen from Figure 15, the origin of the global reference frame was chosen to coincide with the starting point. The positive $x - axis$ was aligned with magnetic North and the positive $y - axis$ aligned with East.

The control gains of (15) were selected as $k_p = \text{diag}[0.5, 0.5, 5.0]$ and $k_e = \text{diag}[30, 30, 40]$ based on simulation and prior testing. Note that the stability analysis in Sect. 4 can be easily extended to positive-definite gain matrices.

Figures 15 and 16 illustrate the tracking performance of the adaptive control system. The "in-the-loop" numerical optimization routines converged in a mean run time of 0.01 seconds. Fig. 20 is representative of the run time in all our experiments, using a 1 Ghz 256 MB RAM Laptop running Windows XP. The worst case run times of up to 0.12 sec tend to occur when there are abrupt fluctuations in the position reported by the GPS. This is because the solution used in the previous iteration is used as an initial guess for the subsequent iteration. When the initial conditions vary gradually the initial guesses are quite accurate and

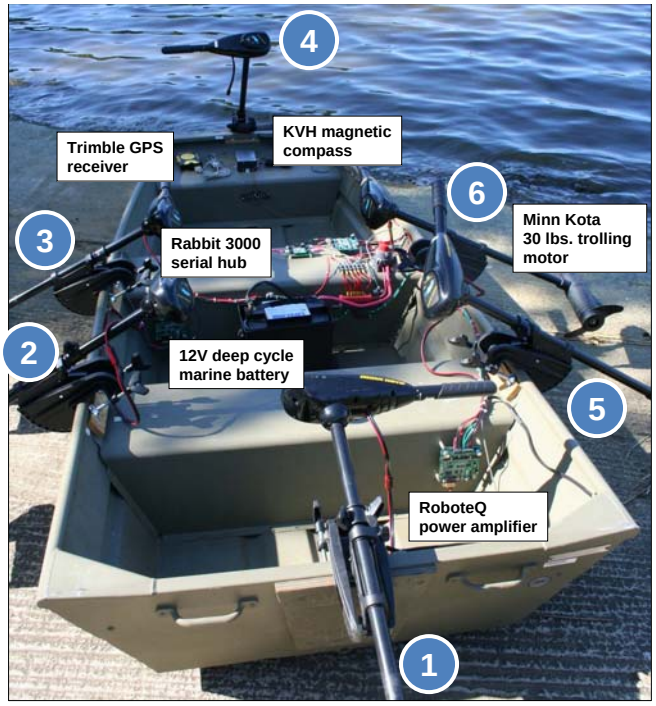

Figure 13: USNA Open-Water Vessel

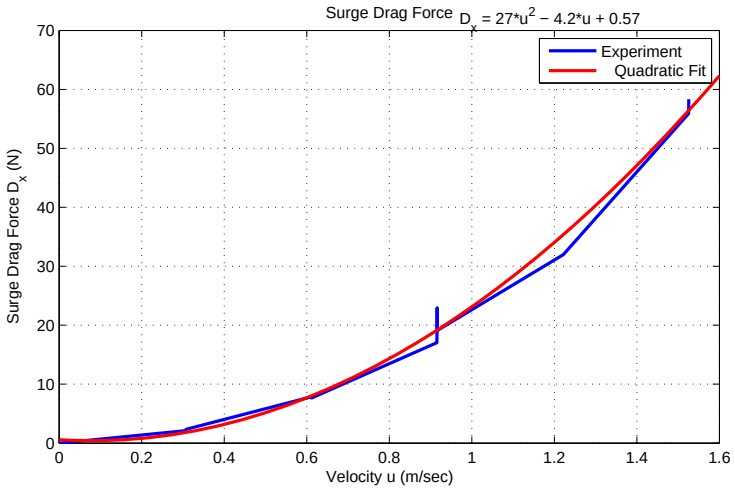

Figure 14: Surge Direction Drag Force.

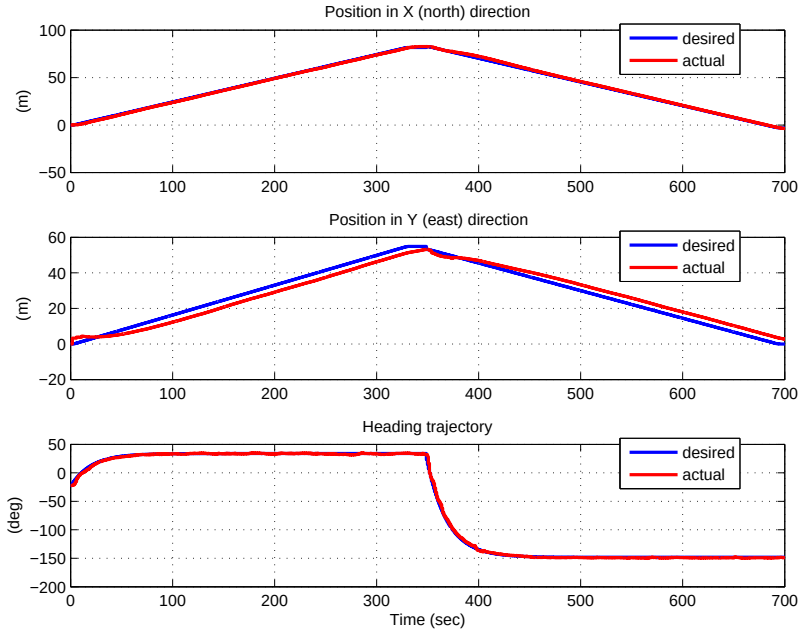

Figure 15: Open-Water Position/Orientation Tracking Results.

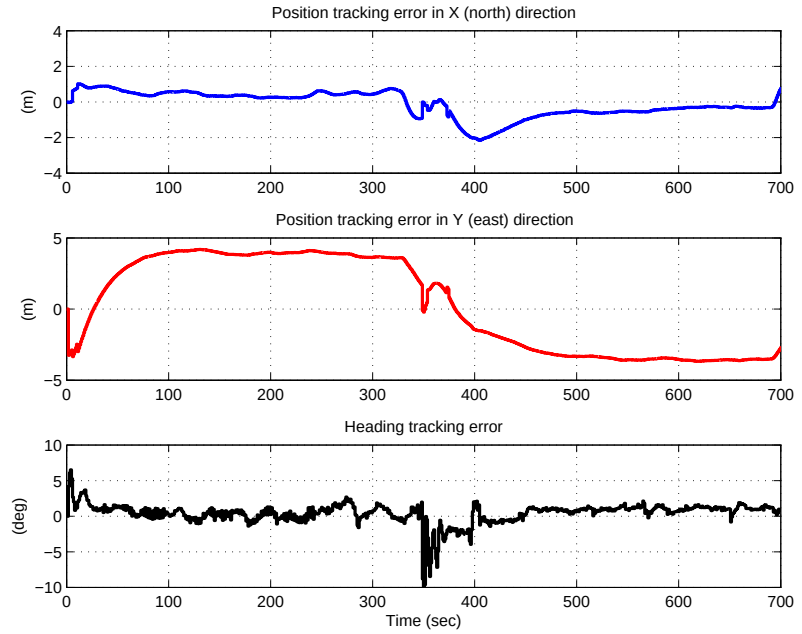

Figure 16: Position/Orientation Tracking Error.

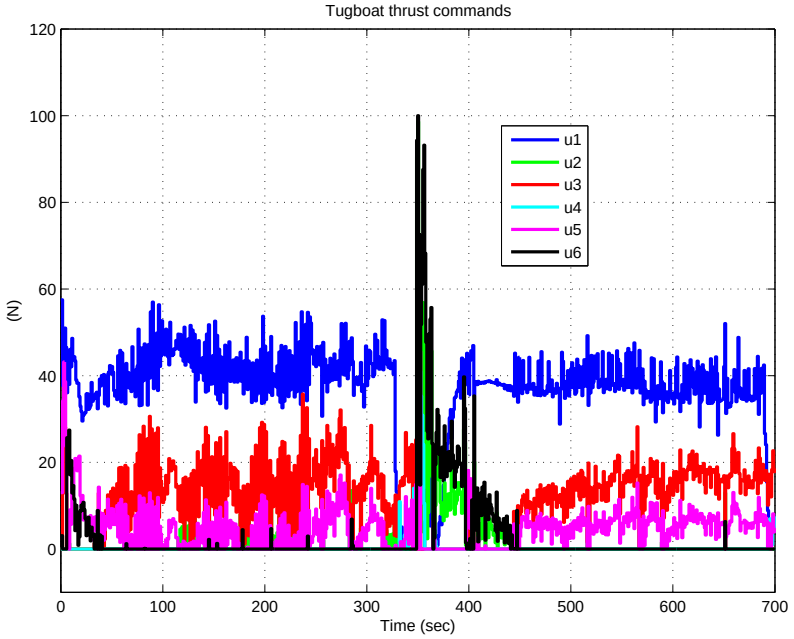

Figure 17: Tugboat Thrust Commands.

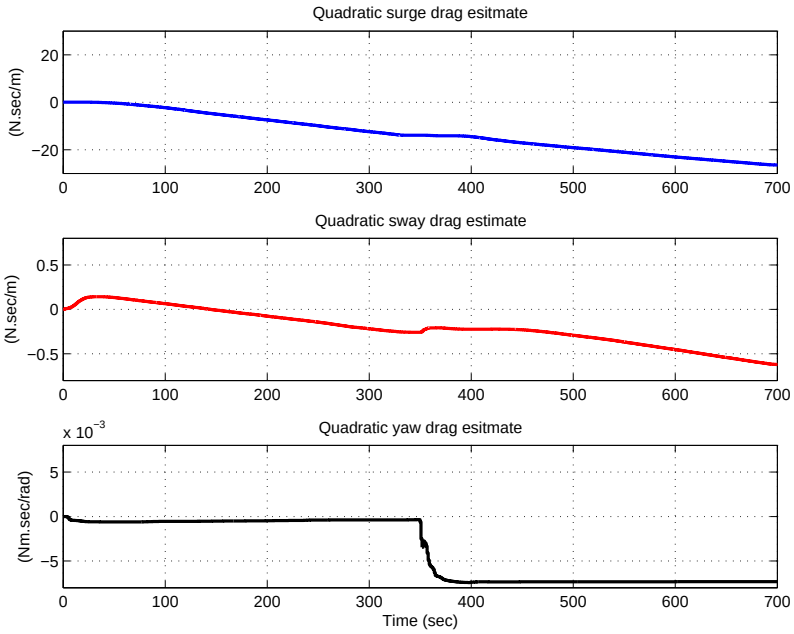

Figure 18: Quadratic Parameter Estimates.

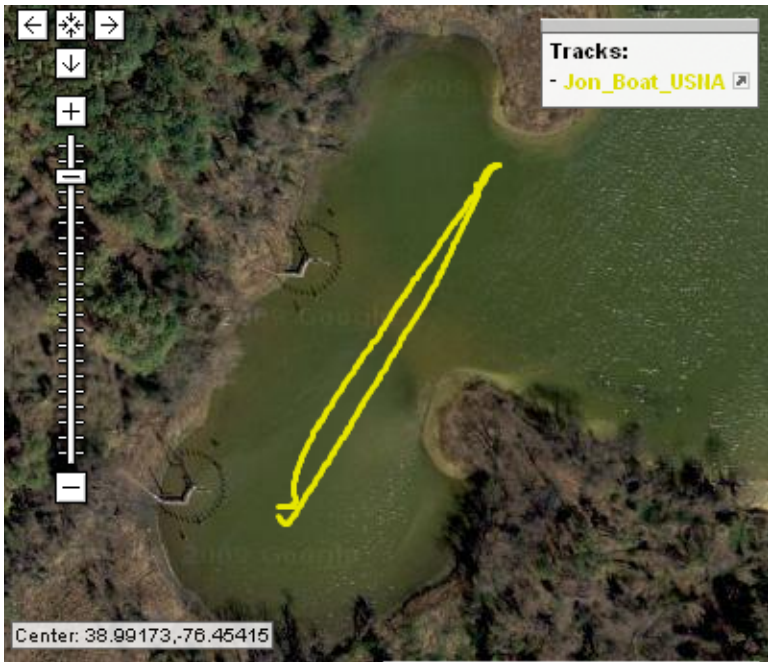

Figure 19: GPS Track of Experimental Vessel Shown in Google Maps.

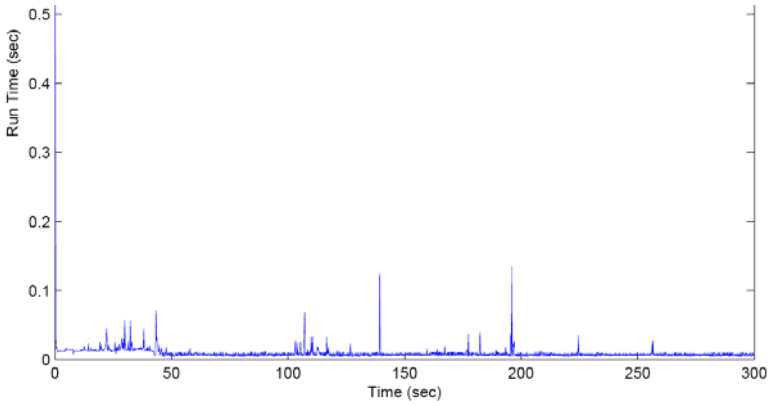

Figure 20: Run time at each iteration of the numerical algorithms used in Thrust Allocation (Sect. 4.3) and Trajectory Generation (Sect. 4.4).

routines converge quickly (ex. 0.01 sec). The code actually specifies an upper bound of 0.15 sec per iteration after which we simply return the bracketed best guess and use the mid-point, this option was never exercised during our any of our experimental trials.

5.4 Discussion of Open-Water Experimental Results

As observed in Figure 16, relatively good position/yaw tracking is achieved despite the experimental vessel being subject to such environmental factors as wind and waves. The vessel is able to track the time parameterized desired trajectory $p_d(t)$ in the x (North) direction to almost within a 1.0 (m) meter and within approximately 4.0 (m) in the y (East) direction.

In order to generate higher precision position estimates the Trimble Pathfinder GPS requires 5 or more satellites to be in view. Note that there can be large fluctuations or even drop outs in the GPS reported position depending on the actual number of satellites in view (especially the WAAS). In an attempt to address this issue, ...

From Figure 16, one can see that the tracking in the y direction is larger as compared to the x direction. This may be to the fact that the mouth of the inlet in which the experiments were conducted faces east; therefore, the waves induced by other marine traffic travel in addition to the tidal flow move in an east to west fashion thereby produces a constant force on the boat in that direction (i.e., an unmodeled disturbance).

Figure 17, illustrates that the commanded thrusts remain under the maximum force of $133(N)$. Figure 18) shows some sample adaptive estimates of the drag quadratic drag coefficients.

Remark 5.2 *The experimental results presented in Figures 15 through 19 were selected to illustrate the control framework. Approximately 20 field trials have been conducted since July 2008. This testing has led to to some insights on the role of gain selection. For instance, we have observed that the system is rather sensitive to values of* $k_p > 1.0$. *Higher values produced noticeable oscillations in the response not observed in simulation.*

6 Conclusions

This paper presents a comprehensive approach to cooperative force control for marine applications such as a group of autonomous tugboats moving a barge. We assume the boats are already in contact with the barge, that their attachment points are fixed and that their thrust inputs are unidirectional and bounded.

First we generate conservative bang-bang trajectories, that avoid inducing actuator saturation. Next we introduce a high-level tracking controller, which generates the desired net force and moment to drive the tracking error to zero. We address uncertainty in the hydrodynamic model parameters through the use of adaptive terms. We use a Lyapunov-based approach to show stability. Note that the terms must be carefully bounded to avoid actuator saturation. Finally we employ a realtime constrained optimization algorithm to allocate the thrust commands to the individual tugboats. We demonstrated our results in simulation, on an indoor test bed in a controlled environment and finally on a 3 meter boat in open water using GPS and a magnetic compass.

There are several avenues for future work. Note that the adaptive control law can be easily extended to accommodate an unknown mass matrix. An even more useful extension would be to assume there are errors in B, the tug configuration matrix. Alas, the online estimation of the moment arms proves difficult, as an incorrect estimate of their sign can induce instability. Addressing this issue is our current focus. In terms of implementation, a more realistic experiment in which the thrusters and trolling motors are replaced by 6 independent scale model tugboats is also an ongoing effort.

Acknowledgments

This work is supported by ONR grant N001408WR20091. In addition, the authors would also like to thank Norm Tyson, Joseph Bradshaw, Ralph Wicklund, and Bill Lowe of the Systems Engineering Technical Support Division for support throughout the project; Erik T. Smith and Eric Regneir for experimental design; and the Naval Architecture Department of USNA for use of the tow tank facility.

References

Arrichiello, F., Das, J., Heidarsson, H., Sukhatme, G., and Chiaverini, S. (2009). Experiments in autonomous navigation with an under-actuated surface vessel via the null-space based behavioral control. In *IEEE/ASME Conference on Advanced Intelligent Mechatronics*, pages 362–367.

Berge, S. and Fossen, T. (1997). Robust control allocation of overactuated ships: Experiments with a model ship. In *4th IFAC Conf. Maneuvering and Control of Marine Craft*, pages 166–171.

Blanke, M. (1981). *Ship Propulsion Losses Related to Automated Steering and Prime Mover Control*. PhD thesis, Technical University of Denmark.

Bordignon, K. A. and Durham, W. C. (1995). Closed-form solutions to constrained control allocation problem. *AIAA J. Guidance, Contr. Dynam.*, 18(5):1000–1007.

Bouguet, J.-Y. (2009). Matlab camera calibration toolbox. www.vision.caltech.edu /bouguetj/calibDoc.

Boyd, S. and Vandenberghe, L. (2004). *Convex Optimization*. Cambridge University Press.

Braganza, D., Feemster, M., and Dawson, D. (2007). Positioning of large surface vessles using multiple tugboats. In *IEEE American Control Conference*, pages 912–917.

Brown, D. (1971). Close-range camera calibration. *Photogrammetric Engineering*, 37(8):855–866.

Compton, R., Chatterton, H., Hatchell, G., and McGgrath, F. (2008). The us naval academy's new yard partol craft: From concept to delivery. *Naval Engineers Journal*, 99(1):37 – 58.

Esposito, J. (2008). Distributed grasp synthesis for swarm manipulation. In *IEEE Conference on Robotics and Automation*, pages 1489–1494.

Feemster, M., Esposito, J., and Smith, E. (2008). Cooperative manipulation on the water. In *IEEE Conference on Robotics and Automation*, pages 1501–1506.

Fossen, T. and Paulsen, M. (1992). Adaptive feedback linearization applied to steering of ships. In *IEEE Conference on Control Applications*, pages 1088–1093.

Fossen, T. I. (2002). *Marine Control Systems: Guidance Navigation and Control of Ships, Rigs and Underwater Vehciles*. Marine Cybernetics, Trondheim.

Fossen, T. I., Loria, A., and Teel, A. (2001). A theorem for UGAS and ULES of (passive) nonautonomous systems: Robust control of mechanical systems and ships. *Int. J. Robust and Nonlinear Contr.*, 11:95–108.

Harkegard, O. (2002). Efficient active set algorithms for solving constrained least squares problems in aircraft control allocation. In *IEEE Conference on Decision and Control*, pages 1295–1300.

Ijspeert, A., Martinoli, A., Billard, A., and Gambardella, L. (2001). Collaboration through the exploitation of local interactions in autonomous collective robotics: The stick pulling experiment. *Autonomous Robots*, 11(2):149–171.

Johansen, T., Fossen, T., and Berge, S. (2004). Constrained nonlinear control allocation with singularity avoidance using sequential quadratic programming. *IEEE Transactions On Control Systems Technology*, pages 211–216.

Khalil, H. K. (2001). *Nonlinear Systems*. Prentice Hall, New Jersey.

Kube, R. and Bonabeau, E. (2000). Cooperative transport by ants and robots. *Robotics and Autonomous Systems*, 30(1-2):85–101.

Lindegaard, K. and Fossen, T. (2003). Fuel-efficient rudder and propeller control allocation for marine craft: experiments with a model ship. *IEEE Transactions on Control Systems Technology*, 11(6):850–862.

Loria, A., Fossen, T. I., and Panteley, E. (2000). A separation principle for dynamic positioning of ships: Theoretical and experimental results. *IEEE Trans. Contr. Syst. Technol.*, 8:332–343.

Lynch, K. (1999). Locally controllable manipulation by stable pushing. *IEEE Transactions on Robotics and Automation*, 15(2):318–327.

Murray, R., Li, Z., and Sastry, S. (1994). *A Mathematical Introduction to Robotic Manipulation*. CRC Press.

Parker, C., Zhang, H., and Kube, R. (2005). Blind bulldozing: Multiple robot nest construction. In *IEEE/RSJ International Conference on Intelligent Robots and Systems*, pages 2010–2015.

Pereira, G., Kumar, V., and Campos, M. (2004). Decentralized algorithms for multi-robot manipulation via caging. *International Journal of Robotics Research*, 23(7):783–795.

Pettersen, K., Mazenc, F., and Nijmeiejer, H. (2004). Global uniform asymptotic stabilization of an underactuated surface vessel: Experimental results. *IEEE Transactions on Control Systems Technology*, 12(6):891–903.

Rus, D. (1997). Coordinated manipulation of objects in the plane. *Algorithmica*, 19(1):129–147.

Skjetne, R., Fossen, T. I., and Kokotovic, P. V. (2004). Robust output maneuvering for a class of nonlinear systems. *Automatica*, 40(3):373–383.

Smith, E., Feemster, M., Esposito, J., and Nicholson, J. (2007). Swarm manipulation an unactuated surface vessel. In *IEEE Southeastern Symposium on Systems Theory*, pages 16–20.

Song, P. and Kumar, V. (2002). A potential field based approach to multi-robot manipulation. In *IEEE International Conference on Robotics and Automation*, pages 1217–1222.

Sordalen, O. J. (1997). Full scale sea trials with optimal thrust allocation. In *4th IFAC Conf. Maneuvering and Control of Marine Craft*, page 150155.

Sorensen, A. J., Adnanes, A. K., Fossen, T. I., and Strand, J. P. (1997). A new method of thruster control in positioning of ships based on power control. In *Proceedings of the 4th IFAC Conference on Manoeuvring and Control of Marine Craft*, pages 10–12.

Spong, M., Hutchinson, S., and Vidyasagar, M. (2006). *Robot Modeling and Control*. John Wiley and Sons, New York.

Stilwell, D. and Bay, J. (1994). Optimal control for cooperating mobile robots bearinga common load. In *IEEE International Conference on Robotics and Automation*, pages 58–63.

Sudsang, A. and Ponce, J. (2005). A new approach to motion planning for disc shaped objects in the plane. In *IEEE Conference on Robotics and Automation*, pages 1068–1075.

Sugar, T. and Kumar, V. (2002). Control of cooperating mobile manipulators. *IEEE Transactions on Robotics and Automation*, 18(1):94–103.

Wang, Z., Nakano, E., and Takahashi, T. (2003). Solving function distribution and behavior design problem for cooperative object handling by multiple mobile robots. *IEEE Transactions on Systems, Man, and Cybernetics, Part A*, 33(5):537–549.

Webster, W. C. and Sousa, J. (1999). Optimum allocation for multiple thrusters. In *Proc. Int. Soc. Offshore and Polar Engineers Conf.*